frontiers | Frontiers in Marine Science

ORIGINAL RESEARCH
published: 02 June 2022
doi: 10.3389/fmars.2022.905255

Seawater Acidification Exacerbates the Negative Effects of UVR on the Growth of the Bloom-Forming Diatom *Skeletonema costatum*

Futian Li[1,2†], Hangxiao Li[1†], Tianpeng Xu[1], Shihu Li[1] and Juntian Xu[1,3,4]*

[1] Jiangsu Key Laboratory of Marine Bioresources and Environment/Jiangsu Key Laboratory of Marine Biotechnology, Jiangsu Ocean University, Lianyungang, China, [2] Marine Resources Development Institute of Jiangsu, Jiangsu Ocean University, Lianyungang, China, [3] Key Laboratory of Coastal Salt Marsh Ecosystems and Resources Ministry of Natural Resources, Jiangsu Ocean University, Lianyungang, China, [4] Co-Innovation Center of Jiangsu Marine Bio-Industry Technology, Jiangsu Ocean University, Lianyungang, China

OPEN ACCESS

Edited by:
Yuanyuan Feng,
Shanghai Jiao Tong University, China

Reviewed by:
Zou Dinghui,
South China University of Technology, China
Zhiguang Xu,
Ludong University, China

***Correspondence:**
Juntian Xu
jtxu@jou.edu.cn

[†]These authors have contributed equally to this work and share first authorship

Specialty section:
This article was submitted to Global Change and the Future Ocean, a section of the journal Frontiers in Marine Science

Received: *26 March 2022*
Accepted: *06 May 2022*
Published: *02 June 2022*

Citation:
Li F, Li H, Xu T, Li S and Xu J (2022) Seawater Acidification Exacerbates the Negative Effects of UVR on the Growth of the Bloom-Forming Diatom Skeletonema costatum. Front. Mar. Sci. 9:905255. doi: 10.3389/fmars.2022.905255

Climate changes such as seawater acidification caused by rising atmospheric CO_2 and increased ultraviolet radiation (UVR) intensity resulting from shoaling of the upper mixed layer may interact to influence the physiological performance of marine primary producers. But few studies have investigated long-term (>30 days) effects of UVR under seawater acidification conditions, along with less attention on the differential effects of long- and short-wavelength UVA. In the present study, four spectral treatments (>280, >320, >360, and >400 nm) under two pCO_2 levels (400 and 1,000 μatm) were set to investigate the interactive effects of seawater acidification and UVR on the bloom-forming diatom *Skeletonema costatum*. The results showed that UVR decreased growth and effective quantum yield of Photosystem II (PSII) by 9%–16% and 11%–24%, respectively, but it enhanced cell sizes significantly. Long- and short-wavelength UVA showed differential effects on cell volume and the effective quantum yield of PSII, especially at the elevated CO_2 level. Generally, seawater acidification depressed the effective quantum yield of PSII and cell volume by 6%–18% and 8%–39%, respectively. Additionally, the contents of key PSII proteins (D1 and D2) decreased at the elevated CO_2 level. Elevated CO_2 significantly increased the inhibition of UVR on growth in the >280 nm spectral treatment when compared with ambient CO_2, while it showed no effects in other spectral treatments. Overall, the results indicate that the effects of seawater acidification on the ubiquitous diatom are light wavelength-dependent.

Keywords: growth, photosynthetic performances, seawater acidification, *Skeletonema costatum*, UV radiation

INTRODUCTION

The oceans absorb about one-third of the atmospheric CO_2 emitted by anthropogenic activities since the industrial revolution, which leads to ocean acidification (OA) (Sabine et al., 2004). OA is predicted to have significant effects on marine organisms at different trophic levels in the marine ecosystem. Under the OA scenario, seawater pH and CO_3^{2-} concentration decrease, while

concentrations of H^+, HCO_3^-, and aqueous CO_2 increase (Hurd et al., 2019). It is supposed that OA, alongside ocean warming and associated shoaling of the upper mixed layer and decline in nutrient availability, would influence the marine ecosystem dramatically (Bopp et al., 2013). For example, calcifying organisms are considered to be more vulnerable to OA, with decreased calcification rate (Gao et al., 2009; Albright et al., 2016; Li et al., 2021), and varied results were found for non-calcifying organisms due to the complexity of ocean dynamics (Gao and Campbell, 2014). High CO_2 could increase growth rates of some centric diatom species (Wu et al., 2014), while OA could decrease the growth of the oceanic diatom *Thalassiosira oceanica* (Li et al., 2016), and no detectable effects of OA on growth and photosynthesis of the coastal diatom *Thalassiosira weissflogii* were found (Li et al., 2019). In some field studies, enhanced diatom growth was observed in phytoplankton communities when exposed to high CO_2 (Tortell et al., 2008; Feng et al., 2009). However, decreased abundance of microplanktonic diatoms under OA scenario was also reported in an Antarctic coastal community (Hancock et al., 2018). The region-specific and species-specific responses of diatoms to OA documented in previous studies may result from the trade-off between the positive effects of elevated CO_2 and the negative effects of decreased pH (Gao and Campbell, 2014). Despite the varied results, OA generally decreased the photosynthetic affinity for inorganic carbon and thus led to the downregulation of CO_2-concentrating mechanisms (CCMs) in a range of diatoms (Raven and Beardall, 2014). At the projected pCO_2 level at the end of this century (800–1,000 ppmv), the downregulation of CCMs is expected to save 3%–6% of energy for carbon fixation in diatoms (Hopkinson et al., 2011).

Phytoplankton cells are exposed to both photosynthetically active radiation (PAR) and ultraviolet radiation (UVR, including UVA and UVB). UVR is generally considered to have adverse effects on the photosynthesis process of phytoplankton (Bais et al., 2018). The influences would continue because of the long existence of ozone-depleting substances in the atmosphere (Williamson et al., 2014) and shoaling of the upper mixed layer (Bopp et al., 2013). Under excessive PAR and UVR, the reaction center of the PSII protein pigment complex in phytoplankton cells would be damaged by reactive oxygen species (ROS) (Salin, 1988). UVR could also damage membrane proteins (Murphy, 1983), which are related to the operation of CCMs and nutrient uptake. Limited studies have focused on the effects of UVR on CCMs of phytoplankton. Beardall et al. (2002) showed that CCM activity of *Dunaliella tertiolecta* was enhanced by UVB, while UVB depressed the activity of Na^+-dependent bicarbonate transporters of the cyanobacterium *Microcystis* (Song and Qiu, 2007). For nutrient uptake, negative effects of UVB were generally reported, while uptake stimulation was also observed (Aubriot et al., 2004). Phytoplankton have a range of molecular mechanisms to protect themselves from UVR damage. The diatom frustules could attenuate UV radiation and protect cells from UV damage (Ellegaard et al., 2016). Some benthic diatoms were found to increase their antioxidant capacity to detoxify ROS in response to chronic (several days) UV exposure and excessive PAR (Rijstenbil et al., 2000). Some photoprotective pigments accumulated and functioned as sunscreen (Ha et al., 2014), and mycosporyne-like amino acids (MAAs) also accumulated to cope with high light stress (Smith et al., 1992). Although phytoplankton are equipped with these protective mechanisms, significant negative effects caused by UVR have been observed in numerous studies. The UVR tolerance of phytoplankton is different from species to species (De Tommasi et al., 2018), and this may be related to cell size (Wu et al., 2015). Additionally, the UVR effects also depend on the intensity and fluctuation of solar irradiance. Positive effects of UVA on photosynthetic carbon fixation rate of coastal phytoplankton were reported under reduced levels (Gao et al., 2007) or fast-fluctuating solar irradiance (Helbling et al., 2003). UVA has also been shown to be involved in the photorepair process of UVB-induced DNA damage (Buma et al., 2003).

Phytoplankton dwelling in the upper mixed layer are undergoing a series of variations caused by climate changes, such as OA and enhanced UV radiation. As one of the key photosynthetic phytoplankton groups and primary producers in marine ecosystems, diatoms play a vital role in the transfer process of particulate organic material (Tréguer et al., 2018). Independent effects of OA or UVR on marine diatoms have been extensively studied, and some studies have investigated the interactive effects of OA and UV (Beardall et al., 2014). However, most previous studies generally ignore the difference between long- and short-wavelength UVA, which was suggested to have different effects on phytoplankton (Harrison and Smith, 2011). In the present study, we cultured *Skeletonema costatum*, a bloom-forming diatom species, at two pCO_2 levels (400 and 1,000 μatm) to investigate the effects of OA after chronic exposure to four spectral treatments (>280, >320, >360, and >400 nm), with special focus on the differential effects of long- and short-wavelength UVA.

MATERIALS AND METHODS

Culture Conditions

S. costatum was originally isolated from the coastal water of Gaogong Island, Jiangsu province (34.7074°N, 119.4926°E). *S. costatum* cells were precultured under natural solar irradiance, and autoclaved natural seawater enriched with f/2 medium (Guillard and Ryther, 1962) was used for cultures. Seawater was collected from coastal regions of Haizhou Bay, and the mean values of *in situ* nitrate and phosphate concentrations were 14 and 4 μmol l^{-1}, respectively. Precultures were maintained in 500 ml polycarbonate bottles before cells were transferred to quartz tubes in a water tank, and bottles were covered by two layers of neutral-density screens to avoid high light stress and achieve a more realistic light intensity, which was experienced by phytoplankton in the upper mixed layer. Intensities of PAR (400–700 nm), UVA (315–400 nm), and UVB (280–315 nm) were recorded by a broadband solar radiometer (LoggerNet CR3000, Campbell). The culture temperature was controlled at 20°C by a thermostat (HYH-2DR-B, Sunsun).

Experimental Setup

Two pCO_2 levels (400 and 1,000 μatm) and four spectral treatments (>280, >320, >360, and >400 nm) were set, and triplicate cultures were used for each treatment. *S. costatum* was cultured at 20°C in 100-ml quartz tubes and was aerated with sterile ambient air (400 μatm) or CO_2-enriched air (1,000 μatm). All the tubes were cultured in a water tank with two layers of neutral-density screens. The high pCO_2 levels were achieved by a CO_2 plant incubator (HP 1000 G-D, Ruihua). Different light wavelength treatments were realized by using ultraviolet filters that could transmit light with wavelengths above 280, 320, 360, and 400 nm, respectively (**Figure 1**). Cells were diluted with fresh medium every 3 days, and cell concentrations were controlled at less than 2×10^5 cells ml^{-1}. The pH variation caused by cell metabolism was less than 0.05 units. After acclimation for at least 30 days, the following physiological parameters were sampled and measured.

Growth and Cell Volume Measurements

Triplicate samples of all treatments were collected at 24 and 72 h after dilution and were fixed with Lugol's solution to estimate cell density and volume. The plankton counting chamber (DSJ-01, Xundeng) and optical microscope (DM500, Leica) were used to count cells. Specific growth rates of cells were calculated as follows: $\mu = (LnN_t\text{-}LnN_0)/(t\text{-}t_0)$, where N_t represents the cell concentration at time t and N_0 represents the cell concentration at time t_0; in this experiment, $t - t_0 = 2$ d. Cells were photographed with a digital camera (ToupCam, Toup Tek), and the diameter and height of cells were measured by ToupView software, and cell volume was calculated according to the equation for a cylinder.

Chlorophyll *a* and Biogenic Silica Measurements

Each sample of 80 ml for chlorophyll *a* measurement was filtered onto a GF/F filter, and then 4 ml of methanol was added. Chlorophyll *a* was extracted at 4°C overnight in darkness. Then, the absorption values of supernatants at 632, 665, and 750 nm were detected by an ultraviolet spectrophotometer (Ultrospect 3300 pro, Amersham Bioscience). The chlorophyll *a* concentration of *S. costatum* was calculated by the equation of Ritchie (2006).

Each sample of 80 ml for biogenic silica (BSi) measurement was filtered onto a polycarbonate filter (25 mm, Merck Millipore). Filters were then dried at 80°C overnight. BSi on each filter was digested by NaOH neutralized with HCl as previously described (Li et al., 2021). After adding molybdate soln and reducing agent into each tube, the absorption was measured at 810 nm by an ultraviolet spectrophotometer (Ultrospect 3300 pro, Amersham Bioscience) according to Brzezinski and Nelson (1995).

Chlorophyll Fluorescence Measurement

The effective quantum yield of PSII (Fv'/Fm') and rapid light curves (RLCs) were measured by a handheld chlorophyll fluorometer (AquaPen-C, AP-P 100). Cells were concentrated by gentle vacuum filtration, and RLCs were measured at eight light intensities (0, 10, 20, 50, 100, 200, 500, and 1,000 μmol photons m^{-2} s^{-1}) lasting for 10 s each. Samples were acclimated to culture light condition before RLC measurements to avoid an induction effect. Relative electron transport rates (rETR) were estimated as follows: $rETR = PAR \times Fv'/Fm' \times 0.5$, where PAR represents the actinic light intensity (μmol photons m^{-2} s^{-1}); Fv'/Fm' represents the effective quantum yield of PSII; 0.5 is based on the assumption that PSII receives half of all absorbed quanta. RLCs were fitted as follows: $rETR = PAR/(a \times PAR^2 + b \times PAR + c)$, where a, b, and c are model parameters. Then, three parameters were used to calculate the maximum relative electron transport rate ($rETR_{max}$), apparent photon transfer efficiency (α), and light saturation point (I_k) according to Eilers and Peeters (1988).

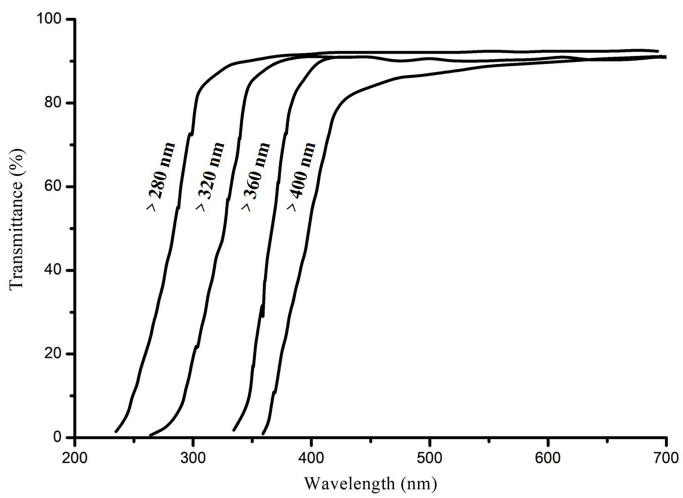

FIGURE 1 | Transmittance spectra of different ultraviolet filters.

Photosynthesis and Respiration Measurements

Photosynthesis vs. light intensity (P-I) curves were measured at 20°C by a Clark-type oxygen electrode (Oxygraph+, Hansatech). Cells were gently concentrated onto cellulose acetate membranes (47 mm, Xinya) and then were resuspended in 5 ml Tris-buffered medium. Respiration rates in darkness and net photosynthetic oxygen evolution rates at eight light intensities (0, 10, 20, 50, 100, 200, 400, 600, and 1,000 μmol photons m^{-2} s^{-1}) were identified. A halogen lamp (QVF135, Philips) was used as the light source, and the increasing light intensities were realized by adjusting the distance between the lamp and the electrode. P-I curves were fitted according to Henley (1993): $P = P_m \times \tanh(\alpha \times PAR/P_m) + R_d$, where P represents photosynthetic rate, P_m represents light-saturated photosynthetic rate, α is apparent photon transfer efficiency, PAR is light intensity, and R_d is dark respiration rate. I_k (light saturation point) and I_c (light compensation point) were calculated as follows:$I_k = P_m / \alpha, I_c = R_d / \alpha$

Protein Measurement

The abundance of PsbA (D1), PsbD (D2), PsbB (CP47), and RbcL proteins of cells in different treatments was quantified as previously described (Li et al., 2021). Briefly, protein samples were separated by sodium dodecyl sulfate polyacrylamide gel electrophoresis (SDS-PAGE) (12%) and were transferred onto polyvinylidene difluoride (PVDF) membranes that were then immersed in blocking solution with antibodies (D1, D2, CP47, Rubisco L; Agrisera) for 1 h, and then goat anti-rabbit secondary antibodies were used. Blots were developed by using an enhanced chemiluminescence (ECL) reagent and were quantified with a chemiluminescence detection system (Tanon 5500, Tanon).

Data Analyses

Data were presented as mean ± SD (standard deviation). Data of specific growth rate were analyzed by a repeated-measures ANOVA. One-way ANOVA was used to detect differences in other parameters among solar spectral irradiance treatments. Tukey test was used for *post-hoc* analysis when *P* values were <0.05. The independent-samples *t*-test was applied to compare differences between two pCO_2 levels. The general linear model was used to assess the interactive effects of CO_2 level and spectral treatment on parameters.

RESULTS

Solar Irradiance

The experiment was conducted in summer time and lasted for about 1 month. During the experimental period, the average solar irradiance at noon in a day could reach 238.41 W m^{-2} (**Figure 2A**), and the maximal total daily doses were found in day 6 (PAR: 10.61 MJ m^{-2}, UVA: 1.17 MJ m^{-2}, UVB: 0.05 MJ m^{-2}), while the minimum values were observed in day 4 (PAR: 1.77 MJ m^{-2}, UVA: 0. 20 MJ m^{-2}, UVB: 0.01 MJ m^{-2}; **Figure 2B**). Two layers of neutral-density screens filtered out about 60% of solar irradiance.

Growth Rate and Cell Volume

The specific growth rates in different treatments ranged from 1.50 ± 0.12 to 1.94 ± 0.10 d^{-1}. The growth rate of cells in the PAR treatment (>400 nm) was significantly higher than that in other treatments regardless of CO_2 treatments, except for no significant difference between >360 and >400 nm spectral treatments at the elevated CO_2 level (**Figure 3**). Compared with cells in the >400 nm spectral treatment, cells exposed to UVR showed 9%–16% lower growth rate. In the same spectral treatment, high CO_2 always showed no effects on growth of *S. costatum* cells. However, HC cells in the >280 nm spectral treatment showed 12% lower growth rate than LC ones ($P = 0.007$).

UVR significantly increased the cell volume of *S. costatum* at both CO_2 levels (**Figure 4**). At ambient CO_2 levels, cells in the >360 nm spectral treatment had much smaller volumes than those of the >320- and >280 nm spectral treatments ($P < 0.05$), and cells in the PAR treatment had the smallest volume. Cells at the high CO_2 level showed a similar trend as those at ambient CO_2 levels, except for no significant difference between >360 and >400 nm spectral treatments. Elevated CO_2 decreased cell sizes in all treatments except for the >400 nm spectral treatment ($P = 0.001$, $P = 0.002$, $P = 0.009$ for the >280, >320, and >360 nm spectral treatments, respectively). CO_2 level and spectral treatment had a notable interaction on cell volume ($P = 0.002$).

Chlorophyll *a* and Biogenic Silica Contents

At ambient CO_2 levels, chl *a* content of cells in the >280 nm spectral treatment was significantly lower than that in other treatments ($P < 0.05$), while there were no significant differences among the four spectral treatments at the elevated CO_2 level (**Figure 5A**). Elevated CO_2 resulted in higher chl *a* content in all spectral treatments ($P < 0.05$). The CO_2 level and spectral treatment had a notable interaction on chl *a* content ($P = 0.025$).

The BSi contents were unaltered by the spectral treatments, except for the lower content in cells treated by the >280 nm spectral treatment than that of >400 nm spectral treatment at the elevated CO_2 level (**Figure 5B**). Elevated CO_2 had no significant effect on BSi contents for the same spectral treatment.

Chlorophyll Fluorescence

The effective quantum yield of PSII (Fv'/Fm') significantly increased when short wavelengths were cut off (**Figure 6**) at both CO_2 levels, and the highest value was observed in the >400 nm spectral treatment (LC = 0.70 ± 0.01, HC = 0.66 ± 0.01). For the same spectral treatment, high CO_2 significantly reduced Fv'/Fm' by 6%–18% ($P < 0.001$). The CO_2 level and spectral treatment had a notable interaction on Fv'/Fm' ($P < 0.001$).

Different spectral treatments had no significant effects on I_k (light saturation point), α (apparent photon transfer efficiency), and $rETR_{max}$ (the maximum relative electron rate) at both CO_2 levels (**Figure 7** and **Table 1**), except for the lower I_k in the >400 nm spectral treatment compared with the >320 nm spectral treatment at the high CO_2 level. High CO_2 significantly decreased the α value in the >320 nm spectral treatment ($P = 0.04$) and decreased $rETR_{max}$ and I_k in the >400 nm treatment ($P = 0.020$, $P = 0.023$, respectively).

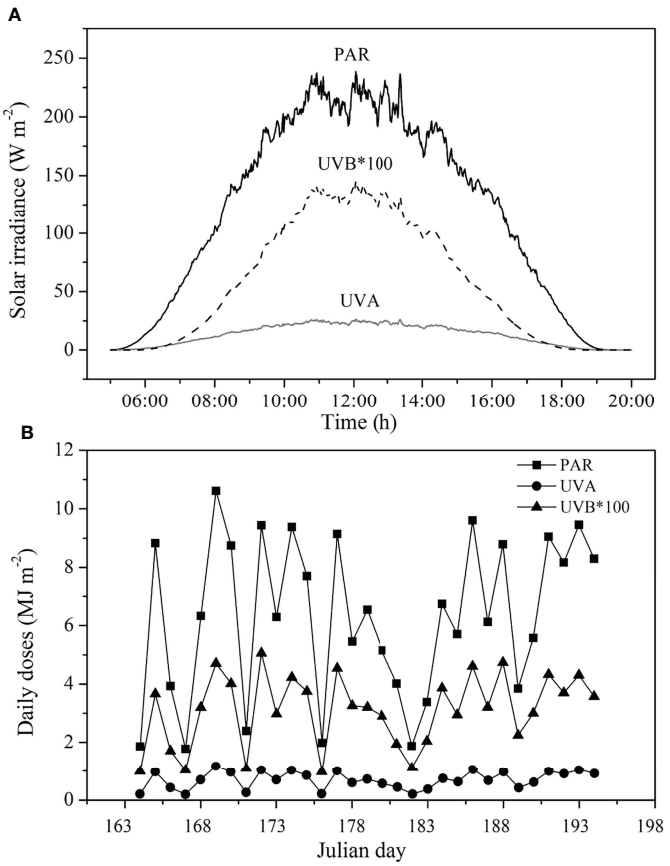

FIGURE 2 | Average irradiance levels **(A)** and daily doses of **(B)** of PAR, UVA, and UVB during the experiment period. PAR, photosynthetically active radiation; UVA, ultraviolet A; UVB, ultraviolet B.

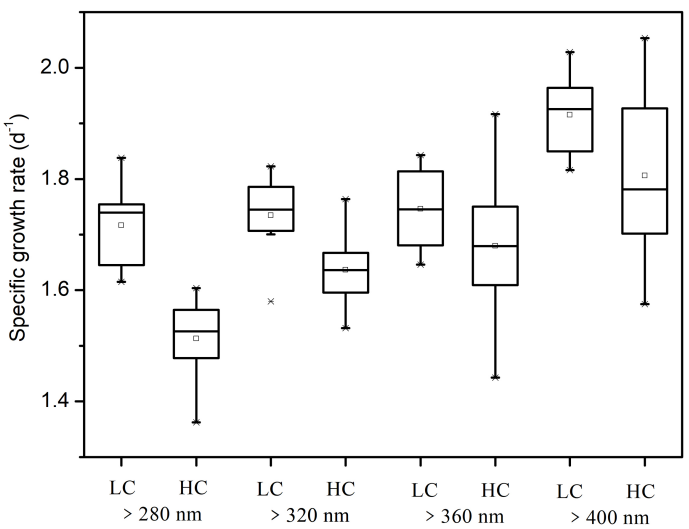

FIGURE 3 | Specific growth rate of *S. costatum* acclimated to ambient (LC) and elevated CO_2 (HC) in different spectral treatments.

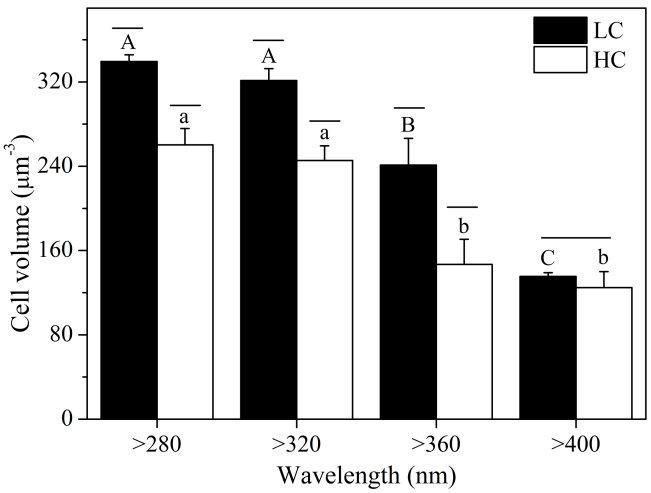

FIGURE 4 | Cell volume of *S*. costatum acclimated to ambient (LC, black bars) and elevated CO_2 (HC, white bars) in different spectral treatments. The different uppercase and lowercase letters represent significant differences between different spectral treatments under LC and HC conditions, respectively.

Photosynthesis and Respiration

According to P-I curves, the maximum photosynthetic rate (P_m), dark respiration rate (R_d), and other parameters were calculated (**Figure 8**). At ambient CO_2 levels, the highest P_m was observed in cells treated by the >400 nm spectral treatment and was significantly higher than that in the >320 nm spectral treatment ($P < 0.05$, **Table 1**). The lowest R_d was also observed in cells treated by the >400 nm spectral treatment, which was significantly lower than that of >280 and >360 nm spectral treatments ($P < 0.05$). The highest values of I_k and I_c were

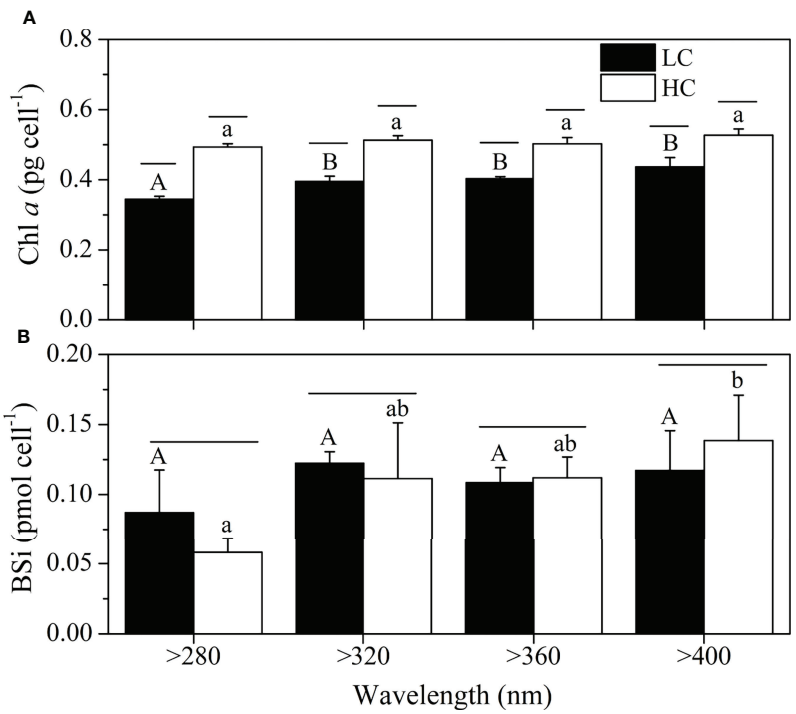

FIGURE 5 | Chla **(A)** and BSi contents **(B)** of *S. costatum* acclimated to ambient (LC, blackbars) and elevated CO2 (HC, whitebars) in different spectral treatments. The different uppercase and lowercase letters represent significant differences between different spectral treatments under LC and HC conditions, respectively.

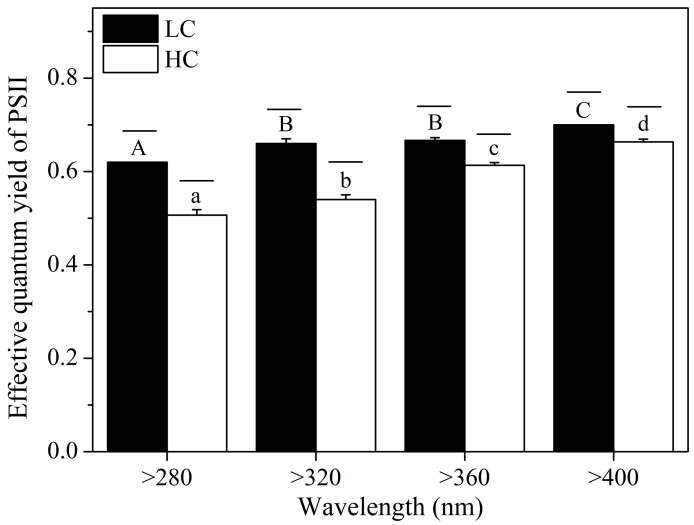

FIGURE 6 | The effective quantum yield of PSII (Fv'/Fm') of *S. costatum* acclimated to ambient (LC, black bars) and elevated CO_2 (HC, white bars) in different spectral treatments. The different uppercase and lowercase letters represent significant differences between different spectral treatments under LC and HC conditions, respectively.

both detected in the >360 nm spectral treatment. At elevated CO_2 levels, there were no significant differences in all of these parameters among the four spectral treatments. Elevated CO_2 significantly decreased P_m by 9% in the >280 nm spectral treatment ($P = 0.01$). Elevated CO_2 significantly enhanced R_d in all spectral treatments except for the >400 nm spectral treatment. Similarly, the I_c was also enhanced in all spectral treatments ($P < 0.05$).

Protein Concentrations

Generally, spectral treatment showed no significant effect on the abundance of these key proteins. Elevated CO_2 decreased the D1 and D2 protein contents, while it did not change the contents of CP47 and RbcL, with the exception that cells grown at elevated CO_2 levels had lower CP47 contents than those at ambient CO_2 levels for the >360 nm spectral treatment (**Figure 9**).

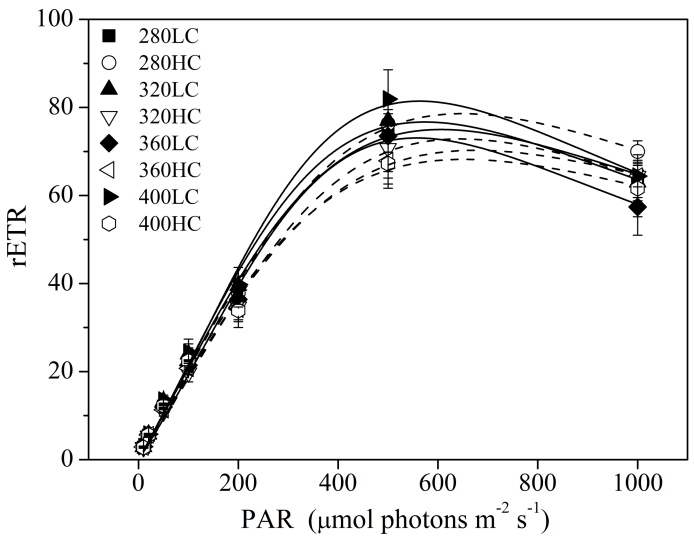

FIGURE 7 | The RLCs of *S. costatum* acclimated to ambient (LC, black bars) and elevated CO_2 (HC, white bars) in different spectral treatments.

TABLE 1 | Photosynthetic parameters of P-I and rapid light curves for *S. costatum* acclimated to ambient and elevated CO_2 in different spectral treatments.

Treatments	I_k (rETR) (μmol photons m^{-2} s^{-1})	α (rETR)	$rETR_{max}$	P_m (pmol O_2 $cell^{-1}$ h^{-1})	α*100	R_d (pmol O_2 $cell^{-1}$ h^{-1})	I_k (μmol photons m^{-2} s^{-1})	I_c (μmol photons m^{-2} s^{-1})
280LC	381 ± 102^{A}	0.21 ± 0.05^{A}	75 ± 4^{A}	0.78 ± 0.02^{AB}*	0.6 ± 0.1^{A}	0.09 ± 0.02^{A}*	133 ± 13^{A}	15 ± 3^{AC}*
280HC	399 ± 11^{ab}	0.20 ± 0.01^{a}	79 ± 2^{a}	0.71 ± 0.02^{a}	0.5 ± 0.1^{a}	0.20 ± 0.02^{a}	131 ± 17^{a}	37 ± 3^{a}
320LC	372 ± 40^{A}	0.21 ± 0.01^{A}*	77 ± 11^{A}	0.56 ± 0.18^{A}	0.4 ± 0.1^{A}	0.04 ± 0.02^{BC}*	147 ± 12^{A}	9 ± 2^{BC}*
320HC	413 ± 34^{a}	0.18 ± 0.02^{a}	73 ± 5^{a}	0.94 ± 0.24^{a}	0.5 ± 0.2^{a}	0.29 ± 0.14^{a}	174 ± 16^{a}	51 ± 12^{a}
360LC	419 ± 66^{A}	0.18 ± 0.03^{A}	73 ± 4^{A}	0.84 ± 0.11^{AB}	0.4 ± 0.1^{A}	0.07 ± 0.03^{AC}*	213 ± 25^{B}	17 ± 4^{A}*
360HC	370 ± 27^{ab}	0.19 ± 0.02^{a}	70 ± 5^{a}	1.01 ± 0.10^{a}	0.6 ± 0.2^{a}	0.28 ± 0.11^{a}	192 ± 68^{a}	49 ± 3^{a}
400LC	419 ± 37^{A}*	0.20 ± 0.02^{A}	81 ± 1^{A}*	0.92 ± 0.13^{B}	0.5 ± 0.1^{A}	0.01 ± 0.01^{B}	186 ± 30^{AB}	2 ± 2^{B}*
400HC	340 ± 10^{b}	0.20 ± 0.01^{a}	68 ± 6^{a}	0.98 ± 0.32^{a}	0.7 ± 0.4^{a}	0.30 ± 0.19^{a}	150 ± 36^{a}	39 ± 17^{a}

Ik (rETR) is light saturation point obtained from RLCs, α (rETR) is apparent photon transfer efficiency obtained from RLCs, rETRmax is maximum relative electron transport rate, P_m is light-saturated photosynthetic rate, α is apparent photon transfer efficiency, R_d is dark respiration rate, I_k is light saturation point, I_c is light compensation point. Asterisks represent significant differences ($P < 0.05$) between two CO_2 levels under the same spectral treatment (t-test). Different letters represent significant differences ($P < 0.05$) between different spectral treatments at the same CO_2 level (Uppercase letters for LC treatment, lowercase letters for HC treatment).

DISCUSSION

Effects of UVR on Growth and Photosynthesis of *S. costatum*

In the present study, UVR decreased the specific growth rate of *S. costatum* by 9%–16%. At ambient CO_2 levels, no significant differences were observed among the spectral treatments with wavelengths shorter than 400 nm. It means that UVB did not exacerbate the negative effects of short- and long-wavelength UVA at ambient CO_2 levels. This may be caused by the low UVB dose in the present study, as we added two layers of neutral-density screens. Effects of UVR (specially UVA) are supposed to be dose-dependent (Gao et al., 2007). For coastal phytoplankton assemblages of the South China Sea, the irradiance thresholds at which the effects of UVR shift from positive to negative are reported in the ranges of 37.2–50.1 W m^{-2} and 1.76–2.33 W m^{-2} for UVA and UVB, respectively (Gao et al., 2007). In the present study, the mean UVA (6.4 W m^{-2}) and UVB (0.28 W m^{-2}) irradiances were under the lower limited values. However, no positive effects of UVR were observed in the present study. This may be related to the species-specific tolerance to high light (Key et al., 2010) and UVR (Wu et al., 2015). The reduced growth rate was accompanied by the increased cell volume in cells exposed to

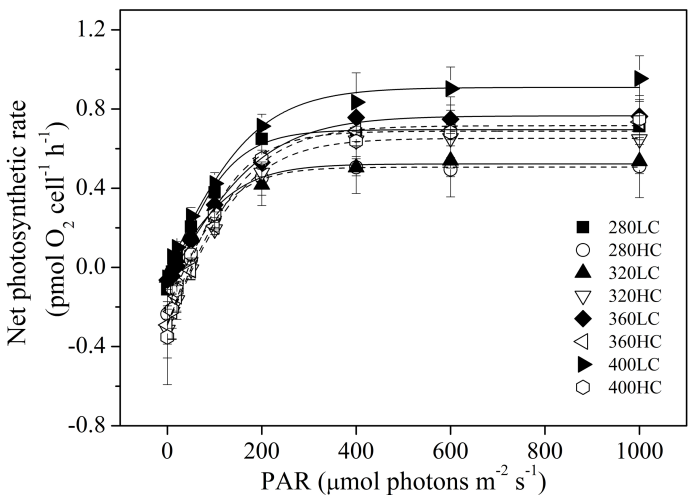

FIGURE 8 | Photosynthesis-light curves (P-I curves) of *S. costatum* acclimated to ambient (LC, black bars) and elevated CO_2 (HC, white bars) in different spectral treatments.

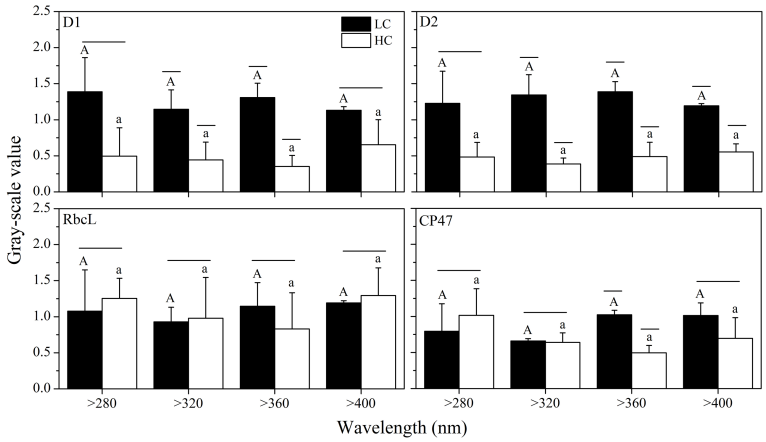

FIGURE 9 | Quantitative analysis of proteins of *S. costatum* acclimated to ambient (LC, black bars) and elevated CO_2 (HC, white bars) in different spectral treatments. The different uppercase and lowercase letters represent significant differences between different spectral treatments under LC and HC conditions, respectively.

UVR treatments. Nahon et al. (2010) also found that the *S. costatum* cells exposed to UVR were about twice the biovolume of the control cells. This means that, in the presence of UVR, the thickness of silicified cell wall became thinner given the unaltered BSi content per cell and markedly increased cell volume.

The effective quantum yield of PSII of *S. costatum* cells was depressed by UVR by 11%. However, this did not indicate the irreversible damage of PSII system by UVR, as shown by the unaltered $rETR_{max}$ and D1 and D2 protein abundance. Similarly, there were no differences in the light-saturated photosynthetic rate (determined under PAR) between cells exposed to >280 and >400 nm spectral treatments. As mentioned above, this may be partly related to the low UVB used during the experimental period. Additionally, the stimulated activity of extracellular carbonic anhydrase of *S. costatum* cells may also play a part (Wu and Gao, 2009).

Long- and short-wavelength UVA showed differential effects on cell volume and the effective quantum yield of PSII of *S. costatum*, especially at elevated CO_2 levels. Cells treated by short-wavelength UVA had lower effective quantum yield and larger cell sizes than cells in the long-wavelength UVA treatment. The differential effects of long- and short-wavelength UVA were also reported in both marine (Mengelt and Prézelin, 2005) and freshwater phytoplankton communities (Harrison and Smith, 2011). It is reasonable to assume that the difference in inhibition effects between long- and short-wavelength UVA will be enlarged with the UVR irradiance increases. As the short-wavelength UVR attenuates more rapidly with depth in most water bodies, and dissolved organic matter influences the attenuation coefficient of UVR (Kirk, 1994), the effects of UVR could be depth-dependent and be related to the concentration of organic matter in water columns. Thus, it is important to investigate the effects of long-wavelength UVR and consider the distinct light environment at different water depths in further studies.

Interactive Effects of Ocean Acidification and Spectral Exposure

Cells grown in HC treatment always showed lower growth rates than those of LC population, with increasing respiration but smaller cell size. This might be related to the high energy cost for cells to maintain intracellular acid–base homeostasis (Raven, 2011). In all spectral treatments, elevated CO_2 significantly decreased the contents of D1 and D2 protein, which includes both photochemically active PSII and PSII that is inactivated but retains D1 and D2 subunits. This was in line with the lower effective quantum yield of PSII at higher CO_2. Along with the faster removal of PsbA from a pool of photoinactivated PSII centers (Gao et al., 2018), elevated CO_2 could alter the dynamic balance of photoinactivation and repair of PSII.

The impacts of elevated CO_2 on *S. costatum* depended on light wavelengths, as shown by the changes in specific growth rate. Elevated CO_2 significantly exacerbated the inhibition of UVR on growth in the >280 nm spectral treatment when compared with ambient CO_2, while it showed no effects in other spectral treatments. This indicates that elevated CO_2 exacerbates the negative effects of UVB on the growth of *S. costatum*. Similarly, the diatom *Thalassiosira pseudonana* was more sensitive to UVR (UVA: 6.91 W m^{-2}; UVB: 0.44 W m^{-2}) after being acclimated to elevated CO_2 for 7–10 days (Sobrino et al., 2008). However, increased CO_2 partly counteracted the UVB (1.2 W m^{-2})-induced damage on *Phaeodactylum tricornutum* (Li et al., 2012). The inconsistency seems to be related to the UVR dose used and CCM efficiency of species tested in studies. UVB was shown to have species-specific effects on CCMs of different phytoplankton (Beardall et al., 2002; Song and Qiu, 2007), which could influence the energy budget of cells.

The negative effects of increased CO_2 on growth of *S. costatum* were found when light intensity was higher than 178 μmol photons m^{-2} s^{-1} (Gao et al., 2012). In the present study, the effective quantum yield of PSII was 6% lower at elevated CO_2 levels compared with ambient CO_2 levels, while no effects of CO_2 on growth were detected in this spectral treatment due to the large variations. Dynamic light could impose extra stress on the photosynthetic apparatus, resulting in decreased growth and carbon fixation rates compared with constant light (Hoppe et al., 2015). Thus, it should be worth noting that the results obtained under constant light condition cannot be simply extrapolated to real oceans. Additionally, the effects of elevated CO_2 were shown to be modulated by other factors, such as nutrient availability (Hong et al., 2017), temperature (Taucher et al., 2015), competition with other photoautotrophs (Gao et al., 2019), and combination of temperature and photoperiod (Li et al., 2021). It is crucial to clarify the interactions of the main environmental factors to make accurate predictions about the effects of climate changes on marine primary producers.

DATA AVAILABILITY STATEMENT

The raw data supporting the conclusions of this article will be made available by the authors without undue reservation.

AUTHOR CONTRIBUTIONS

FL and JX contributed to conception and design of the study. FL, HL, and TX performed the experiments. SL and JX analyzed the data. FL, HL, and JX wrote the first draft of the article. All authors contributed to article revision and read and approved the submitted version.

FUNDING

This work was supported by the "521project" of Lianyungang City (LYG06521202129), China Postdoctoral Science Foundation (2019M661766), Jiangsu Planned Projects for Postdoctoral Research Funds (2021K181B), Lianyungang Postdoctoral Science Foundation Innovation, Jiangsu Institute of Marine Resources Development Program (JSIMR202008), and MEL Visiting Fellowship (MELRS2104), Priority Academic Program Development of Jiangsu Higher Education Institutions.

ACKNOWLEDGMENTS

The authors thank all of the members of N301 for their support for the study.

REFERENCES

Albright, R., Caldeira, L., Hosfelt, J., Kwiatkowski, L., Maclaren, J. K., Mason, B. M., et al. (2016). Reversal of Ocean Acidification Enhances Net Coral Reef Calcification. *Nature* 531, 362–365. doi: 10.1038/nature17155

Aubriot, L., Conde, D., Bonilla, S., and Sommaruga, R. (2004). Phosphate Uptake Behavior of Natural Phytoplankton During Exposure to Solar Ultraviolet Radiation in a Shallow Coastal Lagoon. *Mar. Biol.* 144, 623–631. doi: 10.1007/s00227-003-1229-y

Bais, A. F., Lucas, R. M., Bornman, J. F., Williamson, C. E., Sulzberger, B., Austin, A. T., et al. (2018). Environmental Effects of Ozone Depletion, UV Radiation and Interactions With Climate Change: UNEP Environmental Effects Assessment Panel, Update 2017. *Photochem. Photobiol. Sci.* 17, 127–179. doi: 10.1039/C7PP90043K

Beardall, J., Heraud, P., Roberts, S., Shelly, K., and Stojkovic, S. (2002). Effects of UVB Radiation on Inorganic Carbon Acquisition by the Marine Microalga *Dunaliella Tertiolecta* (Chlorophyceae). *Phycologia* 41, 268–272. doi: 10.2216/i0031-8884-41-3-268.1

Beardall, J., Stojkovic, S., and Gao, K. (2014). Interactive Effects of Nutrient Supply and Other Environmental Factors on the Sensitivity of Marine Primary Producers to Ultraviolet Radiation: Implications for the Impacts of Global Change. *Aquat. Biol.*, 22, 5–23. doi: 10.3354/ab00582

Bopp, L., Resplandy, L., Orr, J. C., Doney, S. C., Dunne, J. P., Gehlen, M., et al. (2013). Multiple Stressors of Ocean Ecosystems in the 21st Century: Projections With CMIP5 Models. *Biogeosciences* 10, 6225–6245. doi: 10.5194/bg-10-6225-2013

Brzezinski, M. A., and Nelson, D. M. (1995). The Annual Silica Cycle in the Sargasso Sea Near Bermuda. *Deep. Sea. Res. Part I.: Oceanogr. Res. Pap.* 42, 1215–1237. doi: 10.1016/0967-0637(95)93592-3

Buma, A. G., Boelen, P., and Jeffrey, W. H. (2003). UVR-Induced DNA Damage in Aquatic Organisms, in UV Effects in Aquatic Organisms and Ecosystems. *R. Soc. Chem.* Cambridge, UK: Royal Society of Chemistry 1, 291–327.

De Tommasi, E., Congestri, R., Dardano, P., De Luca, A. C., Managò, S., Rea, I., et al. (2018). UV-Shielding and Wavelength Conversion by Centric Diatom Nanopatterned Frustules. *Sci. Rep.* 8, 16285. doi: 10.1038/s41598-018-34651-w

Eilers, P., and Peeters, J. (1988). A Model for the Relationship Between Light Intensity and the Rate of Photosynthesis in Phytoplankton. *Ecol. Modell.* 42, 199–215. doi: 10.1016/0304-3800(88)90057-9

Ellegaard, M., Lenau, T., Lundholm, N., Maibohm, C., Friis, S. M. M., Rottwitt, K., et al. (2016). The Fascinating Diatom Frustule—Can it Play a Role for Attenuation of UV Radiation? *J. Appl. Phycol.* 28, 3295–3306. doi: 10.1007/s10811-016-0893-5

Feng, Y., Hare, C. E., Leblanc, K., Rose, J. M., Zhang, Y., DiTullio, G. R., et al. (2009). The Effects of Increased Pco_2 and Temperature on the North Atlantic Spring Bloom: I. The Phytoplankton Community and Biogeochemical Response. *Mar. Ecol. Prog. Ser.* 388, 13–25. doi: 10.3354/meps08133

Gao, K., and Campbell, D. A. (2014). Photophysiological Responses of Marine Diatoms to Elevated CO_2 and Decreased Ph: A Review. *Funct. Plant Biol.* 41, 449–459. doi: 10.1071/FP13247

Gao, G., Fu, Q., Beardall, J., Wu, M., and Xu, J. (2019). Combination of Ocean Acidification and Warming Enhances the Competitive Advantage of Skeletonema Costatum Over a Green Tide Alga, *Ulva Linza*. *Harmful Algae* 85, 101698. doi: 10.1016/j.hal.2019.101698

Gao, K., Ruan, Z., Villafane, V. E., Gattuso, J.-P., and Helbling, E. W. (2009). Ocean Acidification Exacerbates the Effect of UV Radiation on the Calcifying Phytoplankter *Emiliania Huxleyi*. *Limnol. Oceanogr.* 54, 1855–1862. doi: 10.4319/lo.2009.54.6.1855

Gao, G., Shi, Q., Xu, Z., Xu, J., Campbell, D. A., and Wu, H. (2018). Global Warming Interacts With Ocean Acidification to Alter PSII Function and Protection in the Diatom *Thalassiosira Weissflogii*. *Environ. Exp. Bot.* 147, 95–103. doi: 10.1016/j.envexpbot.2017.11.014

Gao, K., Wu, Y., Li, G., Wu, H., Villafane, V. E., and Helbling, E. W. (2007). Solar UV Radiation Drives CO_2 Fixation in Marine Phytoplankton: A Double-Edged Sword. *Plant Physiol.* 144, 54–59. doi: 10.1104/pp.107.098491

Gao, K., Xu, J., Gao, G., Li, Y., Hutchins, D. A., Huang, B., et al. (2012). Rising CO_2 and Increased Light Exposure Synergistically Reduce Marine Primary Productivity. *Nat. Climate Change* 2, 519–523. doi: 10.1038/nclimate1507

Guillard, R. R. L., and Ryther, J. H. (1962). tudies of Marine Planktonic Diatoms: I. *Cyclotella Nana* Hustedt, and *Detonula Confervacea* (Cleve) Gran. *Can. J. Microbiol.* 8, 229–239. doi: 10.1139/m62-029

Ha, S.-Y., La, H. S., Min, J.-O., Chung, K.-H., Kang, S.-H., and Shin, K.-H. (2014). Photoprotective Function of Mycosporine-Like Amino Acids in a Bipolar Diatom (*Porosira Glacialis*): Evidence From Ultraviolet Radiation and Stable Isotope Probing. *Diatom. Res.* 29, 399–409. doi: 10.1080/0269249X.2014.894945

Hancock, A. M., Davidson, A. T., McKinlay, J., McMinn, A., Schulz, K. G., and Enden, R. L. (2018). Ocean Acidification Changes the Structure of an Antarctic Coastal Protistan Community. *Biogeosciences* 15, 2393–2410. doi: 10.5194/bg-15-2393-2018

Harrison, J. W., and Smith, R. E. (2011). The Spectral Sensitivity of Phytoplankton Communities to Ultraviolet Radiation-Induced Photoinhibition Differs Among Clear and Humic Temperate Lakes. *Limnol. Oceanogr.* 56, 2115–2126. doi: 10.4319/lo.2011.56.6.2115

Helbling, E. W., Gao, K., Gonçalves, R. J., Wu, H., and Villafañe, V. E. (2003). Utilization of Solar UV Radiation by Coastal Phytoplankton Assemblages Off SE China When Exposed to Fast Mixing. *Mar. Ecol. Prog. Ser.* 259, 59–66. doi: 10.3354/meps259059

Henley, W. J. (1993). Measurement and Interpretation of Photosynthetic Light-Response Curves in Algae in the Context of Photoinhibition and Diel Changes. *J. Phycol.* 29, 729–739. doi: 10.1111/j.0022-3646.1993.00729.x

Hong, H., Li, D., Lin, W., Li, W., and Shi, D. (2017). Nitrogen Nutritional Condition Affects the Response of Energy Metabolism in Diatoms to Elevated Carbon Dioxide. *Mar. Ecol. Prog. Ser.* 567, 41–56. doi: 10.3354/meps12033

Hopkinson, B. M., Dupont, C. L., Allen, A. E., and Morel, F. M. (2011). Efficiency of the CO_2-Concentrating Mechanism of Diatoms. *Proc. Natl. Acad. Sci.* 108, 3830–3837. doi: 10.1073/pnas.1018062108

Hoppe, C. J., Holtz, L. M., Trimborn, S., and Rost, B. (2015). Ocean Acidification Decreases the Light-Use Efficiency in an Antarctic Diatom Under Dynamic But Not Constant Light. *New Phytol.* 207, 159–171. doi: 10.1111/nph.13334

Hurd, C. L., Beardall, J., Comeau, S., Cornwall, C. E., Havenhand, J. N., Munday, P. L., et al. (2019). Ocean Acidification as a Multiple Driver: How Interactions Between Changing Seawater Carbonate Parameters Affect Marine Life. *Mar. Freshw. Res.* 71, 263–274. doi: 10.1071/MF19267

Key, T., McCarthy, A., Campbell, D. A., Six, C., Roy, S., and Finkel, Z. V. (2010). Cell Size Trade-Offs Govern Light Exploitation Strategies in Marine Phytoplankton. *Environ. Microbiol.* 12, 95–104. doi: 10.1111/j.1462-2920.2009.02046.x

Kirk, J. T. O. (1994). *Light and Photosynthesis in Aquatic Ecosystems* (Cambridge, UK: Cambridge University Press).

Li, F., Fan, J., Hu, L., Beardall, J., and Xu, J. (2019). Physiological and Biochemical Responses of *Thalassiosira Weissflogii* (Diatom) to Seawater Acidification and Alkalization. *ICES J. Mar. Sci.* 76, 1850–1859. doi: 10.1093/icesjms/fsz028

Li, Y., Gao, K., Villafañe, V. E., and Helbling, E. W. (2012). Ocean Acidification Mediates Photosynthetic Response to UV Radiation and Temperature Increase in the Diatom *Phaeodactylum Tricornutum*. *Biogeosciences* 9, 3931–3942. doi: 10.5194/bg-9-3931-2012

Li, F., Wu, Y., Hutchins, D. A., Fu, F., and Gao, K. (2016). Physiological Responses of Coastal and Oceanic Diatoms to Diurnal Fluctuations in Seawater Carbonate Chemistry Under Two CO_2 Concentrations. *Biogeosciences* 13, 6247–6259. doi: 10.5194/bg-13-6247-2016

Li, F., Xu, J., Beardall, J., and Gao, K. (2021). Diurnally Fluctuating Pco_2 Enhances Growth of a Coastal Strain of Emiliania Huxleyi Under Future-Projected Ocean Acidification Conditions. *ICES J. Mar. Sci.* 78, 1301–1310. doi: 10.1093/icesjms/fsab036

Li, H., Xu, T., Ma, J., Li, F., and Xu, J. (2021). Physiological Responses of Skeletonema Costatum to the Interactions of Seawater Acidification and the Combination of Photoperiod and Temperature. *Biogeosciences* 18, 1439–1449. doi: 10.5194/bg-18-1439-2021

Mengelt, C., and Prézelin, B. B. (2005). UVA Enhancement of Carbon Fixation and Resilience to UV Inhibition in the Genus Pseudo-Nitzschia may Provide a Competitive Advantage in High UV Surface Waters. *Mar. Ecol. Prog. Ser.* 301, 81–93. doi: 10.3354/meps301081

Murphy, T. M. (1983). Membranes as Targets of Ultraviolet Radiation. *Physiol. Plantar.* 58, 381–388. doi: 10.1111/j.1399-3054.1983.tb04198.x

Nahon, S., Charles, F., Lantoine, F., Vétion, G., Escoubeyrou, K., Desmalades, M., et al. (2010). Ultraviolet Radiation Negatively Affects Growth and Food Quality of the Pelagic Diatom Skeletonema Costatum. *J. Exp. Mar. Biol. Ecol.* 383, 164–170. doi: 10.1016/j.jembe.2009.12.006

Raven, J. (2011). Effects on Marine Algae of Changed Seawater Chemistry With Increasing Atmospheric CO_2. *Biol. Envi.: Proc. R. Irish. Acad.* 111, 1–17. doi: 10.3318/BIOE.2011.01

Raven, J. A., and Beardall, J. (2014). CO_2 Concentrating Mechanisms and Environmental Change. *Aquat. Bot.* 118, 24–37. doi: 10.1016/j.aquabot.2014.05.008

Rijstenbil, J., Coelho, S., and Eijsackers, M. (2000). A Method for the Assessment of Light-Induced Oxidative Stress in Embryos of Fucoid Algae via Confocal Laserscan Microscopy. *Mar. Biol.* 137, 763–774. doi: 10.1007/s002270000443

Ritchie, R. J. (2006). Consistent Sets of Spectrophotometric Chlorophyll Equations for Acetone, Methanol and Ethanol Solvents. *Photosynt. Res.* 89, 27–41. doi: 10.1007/s11120-006-9065-9

Sabine, C. L., Feely, R. A., Gruber, N., Key, R. M., Lee, K., Bullister, J. L., et al. (2004). The Oceanic Sink for Anthropogenic CO_2. *Science* 305, 367–371. doi: 10.1126/science.1097403

Salin, M. L. (1988). Toxic Oxygen Species and Protective Systems of the Chloroplast. *Physiol. Plantar.* 72, 681–689. doi: 10.1111/j.1399-3054.1988.tb09182.x

Smith, R. C., Prezelin, B. B., Baker, K. S., Bidigare, R. R., Boucher, N. P., Coley, T., et al. (1992). Ozone Depletion: Ultraviolet Radiation and Phytoplankton Biology in Antarctic Waters. *Science* 255, 952–959. doi: 10.1126/science.1546292

Sobrino, C., Ward, M. L., and Neale, P. J. (2008). Acclimation to Elevated Carbon Dioxide and Ultraviolet Radiation in the Diatom *Thalassiosira Pseudonana*: Effects on Growth, Photosynthesis, and Spectral Sensitivity of Photoinhibition. *Limnol. Oceanogr.* 53, 494–505. doi: 10.4319/lo.2008.53.2.0494

Song, Y., and Qiu, B. (2007). The CO_2 Concentrating Mechanism in the Bloom-Forming Cyanobacterium *Microcystis Aeruginosa* (Cyanophyceae) and Effects of UVB Radiation on its Operation. *J. Phycol.* 43, 957–964. doi: 10.1111/j.1529-8817.2007.00391.x

Taucher, J., Jones, J., James, A., Brzezinski, M. A., Carlson, C. A., Riebesell, U., et al. (2015). Combined Effects of CO_2 and Temperature on Carbon Uptake and Partitioning by the Marine Diatoms *Thalassiosira Weissflogii* and *Dactyliosolen Fragilissimus*. *Limnol. Oceanogr.* 60, 901–919. doi: 10.1002/lno.10063

Tortell, P. D., Payne, C. D., Li, Y., Trimborn, S., Rost, B., Smith, W. O., et al. (2008). CO_2 Sensitivity of Southern Ocean Phytoplankton. *Geophys. Res. Lett.* 35, L04605. doi: 10.1029/2007GL032583

Tréguer, P., Bowler, C., Moriceau, B., Dutkiewicz, S., Gehlen, M., Aumont, O., et al. (2018). Influence of Diatom Diversity on the Ocean Biological Carbon Pump. *Nat. Geosci.* 11, 27–37. doi: 10.1038/s41561-017-0028-x

Williamson, C. E., Zepp, R. G., Lucas, R. M., Madronich, S., Austin, A. T., Ballaré, C. L., et al. (2014). Solar Ultraviolet Radiation in a Changing Climate. *Nat. Climate Change* 4, 434–441. doi: 10.1038/nclimate2225

Wu, Y., Campbell, D. A., Irwin, A. J., Suggett, D. J., and Finkel, Z. V. (2014). Ocean Acidification Enhances the Growth Rate of Larger Diatoms. *Limnol. Oceanogr.* 59, 1027–1034. doi: 10.4319/lo.2014.59.3.1027

Wu, H., and Gao, K. (2009). Ultraviolet Radiation Stimulated Activity of Extracellular Carbonic Anhydrase in the Marine Diatom Skeletonema Costatum. *Funct. Plant Biol.* 36, 137–143. doi: 10.1071/FP08172

Wu, Y., Li, Z., Du, W., and Gao, K. (2015). Physiological Response of Marine Centric Diatoms to Ultraviolet Radiation, With Special Reference to Cell Size. *J. Photochem. Photobiol. B.: Biol.* 153, 1–6. doi: 10.1016/j.jphotobiol.2015.08.035

Conflict of Interest: The authors declare that the research was conducted in the absence of any commercial or financial relationships that could be construed as a potential conflict of interest.

Publisher's Note: All claims expressed in this article are solely those of the authors and do not necessarily represent those of their affiliated organizations, or those of the publisher, the editors and the reviewers. Any product that may be evaluated in this article, or claim that may be made by its manufacturer, is not guaranteed or endorsed by the publisher.